© 2021. Published by The Company of Biologists Ltd.

Intracellular flow cytometric lipid analysis: A multiparametric system to assess distinct lipid classes in live cells

Badwi B. Boumelhem[1], Chelsea Pilgrim[1], Vincent E. Zwicker[2], Jacek L. Kolanowski[2,^], Jia Hao Yeo[3], Katrina A. Jolliffe[2,4], Elizabeth J. New[2,4], Margot L. Day[1], Stephen J. Assinder[1,4*], Stuart T. Fraser[1,3,4,5*]

[1] Discipline of Physiology, School of Medical Sciences
[2] School of Chemistry
[3] Discipline of Anatomy and Histology, School of Medical Sciences
[4] University of Sydney Nano Institute
[5] School of Biomedical Engineering
University of Sydney, Australia.
[^] Current address: Institute of Bioorganic Chemistry, Polish Academy of Sciences, Poznan, Poland
[*] Co-senior authors

Correspondence: Assoc Prof Stuart Fraser
Medical Foundation Building
92-94 Parramatta Road,
Camperdown, NSW, 2050
Phone: +61 2 9036 3313; Fax: +61 2 9036 3316; Email: stuart.fraser@sydney.edu.au

Abstract

The lipid content of mammalian cells varies greatly between cell type. Current methods for analysing lipid components of cells are technically challenging and destructive. Here, we report a facile, inexpensive method to identify lipid content: intracellular flow cytometric lipid analysis (IFCLA). Distinct lipid classes can be distinguished by Nile Blue, Nile Red fluorescence or violet autofluorescence. Nile Blue is fluorescent in the presence of unsaturated fatty acids with a carbon chain length greater than 16. *Cis*-configured fatty acids induce greater Nile Blue fluorescence than their *trans*-configured counterparts. In contrast, Nile Red exhibits greatest fluorescence in the presence of cholesterol, cholesteryl esters, some triglycerides and phospholipids. Multiparametric SPADE analysis of hepatic cellular lipid distribution including Vitamin A autofluorescence is presented. This flow cytometric system allows for the rapid, inexpensive, non-destructive identification of lipid content and highlights the differences in lipid biology between cell types by imaging and flow cytometry.

Journal of Cell Science • Accepted manuscript

Introduction

Lipid metabolism is tightly regulated at the cellular, organ and whole body levels (Frayn *et* al., 2006; Rui, 2011). Lipids are gained from diet or synthesised *de novo* from precursors. Critical lipid classes within mammalian cells include: phospholipids which form cell membranes; free fatty acids (FFA); cholesterol and triglycerides (TAGs); neutral lipids stored in droplets; and lipids involved in inter/intracellular communications such as steroids and phospholipids. Short chain fatty acids (SCFA) such as butyrate regulate gene expression while myristic acid and cholesterol modulate protein function (Astakhova *et* al., 2016; Hu *et* al., 2011).

Rates of obesity, diabetes and metabolic disorders are increasing globally. *In situ* or *in cellulo* detection of lipids by antibody staining is currently ineffective as lipids are typically poor immunogens (Maekawa and Fairn, 2014). Liquid chromatography-mass spectrometry (LC/MS), though highly accurate in determining cellular lipid composition, is destructive (Cespedes *et* al., 2015; Kerwin *et* al., 1996; Murphy and Axelsen, 2011). There is clearly a need for methodologies which allow for the rapid detection of lipid classes in live mammalian cells.

Fluorescent dyes and probes can be useful for lipid detection in cells. Here, we have employed the lipophilic dyes Nile Red (NR) and Nile Blue (NB) to assess differences in neutral lipid and free fatty acid (FFA) composition across a range of tissues (Maekawa and Fairn, 2014). NR and NB are heterocyclic benzophenoxazines (Smith, 1911; Martinez and Henary, 2016). NB is positively charged and contains an iminium group whereas NR is neutral and contains a carbonyl group. NB detects bacterial polyhydroxybutyrate though this staining may be due to NR contamination (Ostle and Holt, 1982). NR is a well-known fluorescent lipophilic stain and has been used to visualise lipid storage in a broad range of cell types from algae to humans (Greenspan *et al*., 1985; Rumin, 2015; McMillian *et al*., 2001; Dates *et al*., 2015). Previously, we demonstrated that NR could distinguish adipocyte heterogeneity at the single cell level by flow cytometry (Boumelhem *et al*., 2017). Fluorescent probes can also be generated to sense specific lipids, including P-IID, which we have recently reported as a sensor for extracellular phosphatidylserine (Zwicker *et al*., 2019).

Here, we report that NB fluorescence is induced by unsaturated FFA with at least 16 carbons. In contrast, NR fluoresces in the presence of cholesterol, cholesterol esters, some triglycerides and phospholipids. This identification of the lipid-specific NB and NR fluorescence, combined with the cell-permeable nature of both dyes has allowed us to utilise these dyes for live cell imaging, histochemistry and flow cytometry, offering new perspectives on the heterogeneity and flux of lipids within mammalian cells. In combination with autofluorescent signals, these lipophilic probes can be used for intracellular flow cytometric lipid analysis (IFCLA).

Journal of Cell Science • Accepted manuscript

Results

Nile Red and Nile Blue are cell-permeable fluorescent lipophilic dyes

The use of NB as a fluorescent stain of mammalian cells has not been extensively reported. Both NR and NB are fluorescent: NR can be excited at 488 nm and emits between 565-640 nm while NB can be excited at 620 nm with emission between 630-700 nm. Cryosections of adult mouse tissues were fixed with 4% paraformaldehyde (PFA) in PBS, incubated with NB and NR, washed and imaged immediately. Confocal microscopy revealed that lipid droplets of brown adipose tissue (BAT) were stained by NR (Fig. 1ai-ii). Laminar structures near the BAT vasculature were also stained with NR (Fig. 1ai, arrowhead). In contrast, NB fluorescence was largely observed in distinct punctate structures within the brown adipocytes (Fig. 1aii, arrowhead). These punctate structures were approximately 1 µm in diameter, stained with NB peripherally and NR centrally and resemble peroxisomes which are abundant in brown adipocytes (Fig. 1aii) (Lodhi and Semenkovich, 2014; Ahlabo and Barnard, 1971; Park *et al*., 2019). Peroxisomes in brown adipocytes are involved in the metabolism of lipids through β- and α-oxidation of very long chain fatty acids and methyl-branched fatty acids (Park *et al*., 2019). NB diffusely stained the cytoplasm of gonadal white adipocytes with fluorescence most intense around the periphery of the cytoplasm (Fig. 1bii). NR intensely stained the lipid droplets of adipocytes in white adipose tissue (WAT) (Fig. 1bii). Compared to BAT, there were less peroxisome-like organelles stained with NB (Fig. 1bii). This could be due to the characteristically large, triglyceride-rich lipid droplet which constitutes much of the cytoplasm in each white adipocyte. Thus, NR and NB can stain distinct intracellular features in brown adipocytes and to a lesser degree, white adipocytes.

To assess the utility of NB for flow cytometry, single cell suspensions of BAT and WAT were prepared with the buoyant fraction (BF) containing adipocytes, and a stromal vascular fraction (SVF) (Boumelhem *et al*., 2017). Cells were incubated with NB and NR and flow cytometry performed. All SVF samples showed a similar pattern with strong NB fluorescence and no or little NR fluorescence demonstrating that NB is cell-permeable and fluoresces in the presence of lipids within mammalian cells (Fig. 1ci-iii, di-iii). In contrast, the buoyant fraction in all tissues studied contained populations with NR and NB. BAT BF cells contained three populations: NR-positive alone (NR^+); NB-positive alone (NB^+) or NR and NB double-positive cells (NR^+NB^+) (Fig. 1civ-vi). NR^+NB^+ cells were larger and more granular compared to those with NR^+ or NB^+ cells which may be indicative of the presence of peroxisomes inside BAT adipocytes (Fig. 1civ-vi). Greater than 90% of buoyant white adipocyte cells were NB^+ (Fig. 1div-vi). Gonadal WAT contained two populations with increasing NB intensity (Fig. 1div-vi). Cells with the greatest NB fluorescence (NB^{++}) were the largest, most granular cells (Fig. 1div-iv). These findings demonstrate that NB and NR can be combined to segregate distinct populations from adipose tissues. However, it is unclear which lipids the two dyes are detecting within these populations.

Journal of Cell Science • Accepted manuscript

Nile Blue and Nile Red lipid specificity

To determine why these structurally similar dyes show distinct lipid detection profiles within cells, spectrofluorimetric analysis of 70 different lipids in PBS was performed (Fig. 2, Table S1. Fig. S4). Neither dye was fluorescent in the presence of saturated fatty acids (Fig. 2a). NB fluoresced only in the presence of specific unsaturated fatty acids (Fig. 2a-c): the monounsaturated fatty acids palmitoleic and oleic acids, which are commonly found in mammalian cells; linoleic acid, which is polyunsaturated and present in mammalian cells and is a precursor of arachidonic acid (Fig. 2a-b). Nervonic acid and erucic acid, which are elongation products of oleic acid, also induced high NB fluorescence.

Of the 22 unsaturated fatty acids assessed, NR fluoresced only in the presence of oleic acid (Fig. 2a). Other unsaturated fatty acids caused NR to fluoresce, but the emission maximum was red-shifted, with peak emission at 620 nm, beyond the range used to detect NR by flow cytometry or confocal microscopy (520 nm – 590 nm, Fig. S3; Fig. S4c). NR fluorescence was observed with cholesterol, cholesteryl esters and triglycerides (Fig. 2a). NR fluorescence was also observed in the presence of low- and high-density lipoproteins (Table S1). NR fluoresced in the presence of phosphatidylcholine (PC), phosphatidylserine (PS), platelet activating factor (PAF) and the brain lipid glucosylceramide (Fig. 2a). PC and PS are components of the mammalian plasma cell membrane lipid bilayer however cell membrane staining has not been observed by histological staining. Neither NR nor NB showed any fluorescent response to the presence of steroids (Table S1). Lipids must contain 16 or more carbons to induce NR or NB fluorescence (Fig. 2a). Small and medium chain fatty acids failed to induce fluorescence in these liquid-based assays. The number and position of double bonds in the fatty acid chain did not significantly influence the observed intensity of NB fluorescence (Fig. 2b, Fig. S1). However, fatty acids with *trans*-configured double bonds, including palmitoleic, oleic, vaccenic, linoleic and eicosapentanoic acids displayed significantly lower fluorescence intensity than their *cis*-configured counterparts of equal carbon number (Fig. 2ci-ii).

To determine whether the spectrofluorimetry data were pertinent to the behaviour of NR and NB in live cells, an array of lipids from multiple classes were added to cultures of mouse embryonic stem (ES) cells for 30 min prior to confocal imaging and flow cytometric analysis. NB fluorescence intensity increased in oleic acid-treated cells but not vehicle (DMSO)-treated cells with diffuse and punctate cytosolic blue staining evident (Fig. 3ai-ii, bi-ii). When assessed by flow cytometry, only mouse ES cells treated with oleic and linoleic acids showed an increase in fluorescence intensity for NB (Fig. 3bi-ii). No change in NB fluorescence intensity was observed for cells treated with saturated fatty acids, cholesterol, cholesterol esters, triglycerides and phospholipids, consistent with our finding above that NB fluorescence is restricted to unsaturated fatty acids (Fig. 2a, 3bi). Therefore, NB exhibits specificity for *cis*-unsaturated FFAs.

Journal of Cell Science • Accepted manuscript

An increase in NR fluorescence was detected in mouse ES cells treated with oleic acid only (P = 0.02) (Fig. 3bii). While NR fluoresces in the presence of cholesterol, cholesterol esters and triglycerides *in vitro* (Fig. 2a), mouse ES cells treated with those lipids did not lead to an increase in NR fluorescence (Fig. 3bii). This could be due to the lack of uptake of these lipids in mouse ES cells due to the short incubation time or alternatively, this could indicate that NR staining of lipid droplets in mouse ES cells is composed mostly of oleic acid (Fig. 3bii).

Dynamic shifts in Nile Red and Nile Blue fluorescence highlight changes in maternal-foetal lipid exchange throughout development

In rodents, the exchange of nutrients between mother and developing embryo takes place at the placental interface and the yolk sac (YS), a membrane that encapsulates the embryo/foetus. The YS is important for the transport of less soluble nutrients such as lipids (Farese *et al*., 1996). NR fluorescence was localised to lipid droplets within the YS at all time points assayed (Fig. 4ai-iii) with fluorescence greatest at embryonic day (E) 10.5 of development and diminished by E18.5 (Fig. 4bi-iii). NB fluorescence was observed in the cytoplasm of YS epithelial cells (Fig. 4bi-iii). Flow cytometry revealed two distinct populations of YS cells: one showing fluorescence of both dyes ($NR^{+}NB^{+}$) and another population which exhibited NB fluorescence alone ($NR^{-}NB^{+}$) (Fig. 4bi-iii, ci-ii). The frequency of $NR^{+}NB^{+}$ cells was greatest at E10.5 (Fig. 4bi, ci, Tables S2 & S3). In contrast, $NR^{-}NB^{+}$ cell frequency was lowest in the earliest developmental stage assayed but significantly increased by E12.5 reaching maximum levels at E15.5 (Fig. 4bi-iii, Tables S2 & S3). At E14.5, there was a clear decline in $NR^{+}NB^{+}$ cells and an increase in $NR^{-}NB^{+}$ cells (Fig. 4cii). Lipid content and transport in the mouse YS therefore dynamically changes throughout development and can be assessed by NB and NR fluorescence intensity.

Nile Blue and Nile Red fluorescence discriminates distinct cell types in adult mouse organs

We next determined whether NR and NB can identify distinct populations in adult mouse tissues. In the adrenal gland, the cortex is composed of steroidogenic cells, whilst the medulla is rich with neuroendocrine chromaffin cells (Rosol *et al*., 2001). Intense NR staining was observed in lipid droplets across all cortical regions of the adrenal gland (Fig. 5ai-ii). NB and NR staining were also observed in the cytoplasm in all cortical regions of the adrenal gland (Fig. 5ai-ii). In contrast, the adrenal medulla showed few if any NR-positive lipid droplets and lower levels of NB fluorescence than the cortex (Fig. 5ai-ii). Flow cytometric analyses revealed that the SVF fraction largely lacks NR fluorescence (Fig. 5bi), suggesting these are predominantly medullary cells, whereas the buoyant fraction is dominated by NR and NB-stained cells, as seen in the cortex (Fig. 5bii). NR and NB fluorescence could therefore be a useful method to isolate these distinct adrenal populations.

The testes contain seminiferous tubules with spermatozoa at different stages of development, supported by the Sertoli cells (Griswold *et al*., 1995; la Torre *et al*., 1976; Hu *et al*., 2010). Within the interstitium between tubules, the Leydig cells synthesise androgens *de novo* from cholesterol (Hu *et al*., 2010). The seminiferous tubules exhibited a low NB signal indicating lower levels of free fatty acids (Fig. 5ci-ii, yellow arrowhead). In contrast, cells distributed

Journal of Cell Science • Accepted manuscript

throughout the interstitium showed intense NR and NB fluorescence (Fig. 5ci-ii, white arrowhead). The size, morphology and location all suggest that these are lipid-rich androgen-producing Leydig cells (Campos-Silva *et al*., 2015; O'Shaughnessy *et al*., 2009) (Fig. 5cii, white arrowheads). The dominant population in the SVF was $NR^{+}NB^{+}$ which is consistent with the fluorescent signal shown by the developing spermatozoa in the lumen of the tubules (Fig. 5di). Flow cytometric analysis of the testes BF showed a complex mixture of cell populations each distinct in their lipid contents (Fig. 5dii). The majority of cells showed moderate levels of NR and NB, but a subset showed 10-fold higher NB fluorescence (Fig. 5dii, $NR^{+}NB^{++}$). Additionally, Leydig cells in histological staining showed the highest levels of NR and NB fluorescence (Fig 5ci-ii, white arrowheads).

Muscle cells contain high levels of free fatty acids

Myocytes require fatty acids to fuel contraction (Zlobine *et al*., 2016). Tile-scan confocal microscopy of sections of entire mouse hearts demonstrated that the cardiac tissue stained predominantly with NB alone (Fig. 6a). Scattered NR^{+} lipid droplets were detected in the left ventricle and the left and right atrium (Fig. 6ai). Correspondingly, both the SVF and BF showed predominantly NB staining by flow cytometry (Fig. 6bi-ii). Together, these data indicate that the cardiac muscle is primarily involved in the metabolism of unsaturated FFA rather than lipid storage. The mouse quadriceps were striking in the variety of NR signals (Fig 6c). All fibres showed NB fluorescence, similar to cardiac muscle, however NR signal varied from fibre to fibre (Fig. 6ci). Muscle fibres that showed higher levels of NB fluorescence also showed NR fluorescence (Fig. 6ci). This segregation of cell types was evident both in the histological staining and in the flow cytometric profiles of the cells in the SVF (Fig. 6di). The BF is composed largely of adipocytes. A $NR^{++}NB^{+}$ population is evident in the flow cytometric analysis of the BF (Fig. 6dii). We attribute this population to the intermuscular adipocytes with the remaining $NR^{+}NB^{+}$ population representing the intramuscular adipocytes (Fig. 6ci, dii). Both cardiac and skeletal muscle are dominated by high FFA levels compared to NR-staining lipid droplets.

Multiparametric flow cytometric analyses of the liver using lipid content to distinguish cell types.

The adult liver is a site of complex lipid metabolism. Retinol, an autofluorescent form of Vitamin A (Vit A) is stored in vacuoles in hepatic stellate cells (HSC) (Higashi *et al*., 2005). The autofluorescent signal of retinol is distinct from NR or NB fluorescence and hence can be included in multiparametric analyses. The large data sets generated by multiparametric flow cytometry can be analysed using Spanning-tree Progression Analysis of Density-Normalised Events (SPADE) analyses (Qiu *et al*., 2011). Vit A-containing cells were located between hepatocytes in close proximity to sinusoidal vessels (Fig. 7a). All HSCs were stained with either NR, NB or both dyes (Fig. 7a). NB and NR staining of the BF of digested liver tissue revealed two populations of varying NB fluorescence (Fig. 7bi-ii). Cells with low NB fluorescence ($NR^{+}NB^{+}$) had two populations (19.2% and 3% respectively) exhibiting Vit A fluorescence (Fig. 7bi-ii). Conversely, cells with brighter NB staining contained a single population (26%) of Vit A+ cells (Fig. 7bi-ii).

Journal of Cell Science • Accepted manuscript

To confirm that the data was suitable for exploratory factor analysis, principal component analysis (PCA) on the data-set was performed. The Kaiser-Meyer-Olkin measure of sampling adequacy (0.711) and Bartlett's test for sphericity (approx X^2 = 705461; *df* = 36; *P<0.001*) fell within the acceptable range. NB and Vit A showed highly significant correlations to all other parameters, while NR was significantly correlated to all parameters except for forward scatter (Table S4). There was a particularly strong correlation between Vit A and NR fluorescence but not between Vit A and NB fluorescence. Spectrofluorimetric analysis demonstrated that NR but not NB fluoresced in the presence of retinol when excited (λ_{max} ~1200 at 488 nm). Retinol alone exhibited fluorescence emission at 405 nm but not 488 nm. The NR signal observed by flow cytometry using the 405 nm excitation laser is therefore most likely indicative of retinol-filled lipid droplets in HSC.

SPADE analyses segregated 16 discrete groups in liver BF cells (Fig. 7ci-ii). A breakdown of the putative cell types for each group can be seen in Figure 7. NR and NB distribution varied across the different groups (Fig. 7ci-ii). In particular, all groups except 14, 15 and 16 exhibited NB fluorescence while only groups 1, 9, 15 and 16 exhibited NR fluorescence (Fig. 7ci-ii). The SPADE plot for Vit A autofluorescence revealed two distinct groups with high levels of fluorescence (Fig. 7ci). Group 16 only contained NR and Vit A fluorescence suggesting differences in HSC maturation stage (Fig. 7ci-ii). These data demonstrate that multiple lipid classes can be assessed by flow cytometry in live cells using commonly available reagents and autofluorescent signals resolving the complex distribution of lipids in cells, tissues and organs.

Discussion

Nile Blue and Nile Red have a long been used as histological stains but their utility as probes of specific lipid classes has not been extensively characterised. Here, we demonstrate that NB is a cell-permeable, far-red probe able to detect the presence of unsaturated FFA with at least 16 carbons, with the *cis* (*Z*-) configuration resulting in higher fluorescence intensity of the dye than the *trans* (*E*-) configuration. In contrast, NR identifies triglycerides, cholesterol and cholesteryl esters but not FFAs. The levels of specificity of both NR and NB allows the identification of biologically important lipids present in mammalian cells when combined. Together with Vit A autofluorescence we have been able to identify characteristic traits of mammalian cell lipid content using non-destructive, non-toxic and relatively inexpensive reagents in a process we term intracellular flow cytometric lipid analysis (IFCLA). In the future, IFCLA can be readily adapted to other lipid-sensing probes such as P-IID, a phosphatidylserine-specific sensor (Zwicker *et al*., 2019).

Changes in cellular lipid content during physiological changes such as exercise, pregnancy, stress and ageing can now be more readily assessed at the single cell level using IFCLA. The FFA demands of cardiac and skeletal myocytes can be monitored by NB fluorescence. Likewise, the lipid contents of hepatic populations could now be more easily investigated. Liver biopsy is commonly used to diagnose non-alcoholic fatty liver disease, the most common cause of abnormal hepatic function among adults (Feldstein *et al*., 2005). While

Journal of Cell Science • Accepted manuscript

liver biopsies are invasive, the sample obtained could be analysed for NB, NR and Vit A autofluorescence by flow cytometry to determine lipid content levels at the single cell level with small amounts of material.

Recently, hyperspectral-stimulated Raman scattering imaging was combined with mass spectrometric analysis of lipids to reveal that ovarian cancer stem cells possess significantly higher levels of unsaturated lipids compared to the non-cancer stem cell population (Li *et al*., 2005). Similar studies could now be performed by flow cytometry using lipophilic probes. Populations of interest could be FACS-purified according to lipid content for cell culture, gene, protein or further lipid analysis. Flow cytometric analysis with NB and NR could potentially be used to accelerate the speed of diagnosis of diseases related to lipid dysmetabolism such as leukodystrophies including Zellweger Syndrome, a peroxisome biogenesis disorder (Klouwer *et al*., 2015), or Niemann-Pick Disease where sphingomyelin or cholesterol are not appropriately metabolised (Peake and Vance, 2010). The IFCLA method that we present here, using comparatively inexpensive probes, endogenous autofluorescence and antibody staining, could help develop the field of flow cytometric lipidomics and potentially assist with improving diagnostic systems.

Acknowledgements
We thank the Bosch Institute Live Cell Analysis Facility for assistance with flow cytometry and the Bosch Institute Advanced Microscopy Facility for assistance with confocal microscopy. This research received no specific grant from any funding agency in the public, commercial or not-for-profit sectors

Methods

Preparation of free fatty acids and lipophilic dyes.

Free fatty acids were reconstituted in nitrogen-purged dimethylsulfoxide (DMSO) to a stock concentration of 100 mmol.L^{-1}. Nile Red (N3013, Sigma Aldrich) was dissolved in DMSO to a stock concentration of 30 mmol.L^{-1}. Nile Blue (N0766, Sigma Aldrich) was dissolved in MilliQ® water to a stock concentration of 10 mmol.L^{-1}.

Spectrofluorometric analyses of Nile Red and Nile Blue in the presence of free fatty acids.

Nile Red and Nile Blue were reconstituted in PBS to a final concentration of 300 nmol.L^{-1} and 1 µmol.L^{-1} respectively. Lipids were pipetted into a 96-well plate to a final concentration of 100 µmol.L^{-1}. PBS containing Nile Red or Nile Blue was then repeatedly pipetted to mix the solution. The plate was inserted into a plate reader (EnSpire, Perkin Elmer) and shaken for 180 s at 60 rpm. Nile Red fluorescence was collected from 510 – 660 nm (l_ex = 488 nm, 5 nm step size) and Nile Blue fluorescence was collected from 620 – 800 nm (l_ex = 600 nm, 5 nm step size). Data was collected and exported with EnSpire Workstation software and analysed using Graphpad Prism v7.0.

Journal of Cell Science • Accepted manuscript

Cell culture of mouse embryonic stem cells

Wild-type, undifferentiated mouse embryonic stem (ES) cells (129SV/J, Kuo *et al*., 2001) were maintained in Dulbecco's Modified Eagle Medium (DMEM) supplemented with 10% (v/v) foetal calf serum (FCS), 2 mM Glutamax™, 1 mM sodium pyruvate, 10,000 $U.mL^{-1}$ penicillin, 10 $mg.mL^{-1}$, streptomycin and 150 µM of 1-thioglycerol. Leukaemia inhibitory factor was added at a concentration of 100 $U.mL^{-1}$ to inhibit spontaneous mouse ES cell differentiation. ES cells were validated by assessing Oct3/4 and Nanog gene expression by qRT-PCR. Germ layer potential is assessed routinely to validate the pluripotent nature of the ES line. Mycoplasma contamination is also assessed routinely and cells have never tested positive.

Confocal imaging of embryonic stem cells

Lipid treated mouse ES cells were washed twice with PBS and then stained with 300 $nmol.L^{-1}$ of Nile Red, 1 $\mu mol.L^{-1}$ of Nile Blue and 0.5 mL of NucBlue for 15 minutes at room temperature. Mouse ES cells were then washed twice with PBS and a cover glass was mounted using VectaShield mounting medium without DAPI (H-1000, Vector Laboratories). The cover glass was sealed using nail polish. Confocal images of lipid treated mouse ES cells were taken on a Leica SPEII equipped with four solid-state lasers (405 nm, 488 nm, 532 nm and 625 nm). Nile Red was excited using the 488 nm laser and Nile Blue was excited using the 625 nm laser. NucBlue was excited using the 405 nm laser. Images were taken on a single plane using an oil-immersed Leica ACS Apochromat 40x objective coupled to the Leica Application Suite – Advanced Fluorescence Software.

Flow cytometry of mouse ES cells

Lipid-treated mouse ES cells were washed twice with PBS followed by addition of 1 mL Cell Dissociation Buffer (ThermoFisher Scientific). Mouse ES cells were then incubated at 37°C for 10 min. An equal volume of PBS with 0.5% (w/v) BSA (FACS buffer) was added to inactivate the Cell Dissociation Buffer. ES cells were centrifuged for 5 minutes at 250 *g*, supernatant was removed and cells re-suspended in 1 mL of FACS buffer. Single cell suspensions of mouse ES cells were stained with 300 $nmol.L^{-1}$ Nile Red and 1 $\mu mol.L^{-1}$ Nile Blue for 15 min. Stained cells were washed with 1 mL of FACS buffer, centrifuged for 5 minutes at 250 *g* and resuspended with FACS buffer containing 0.1% (v/v) propidium iodide and transferred into round bottom FACS tubes. Multi-parametric flow cytometry was performed on a Gallios flow cytometer (Beckman Coulter, Brea, CA, USA) and data collected using the Kaluza G software package. FlowJo V10.1 was used to perform analyses of flow cytometric data.

Mice

Young (8-10 weeks) adult, wild type, outbred Quackenbush Swiss mice (Animal Resource Centre, Perth, Western Australia) were housed in filter top cages. Mice were kept under a 12-hour day-night cycle at constant temperature (21–22°C) and provided food and water *ad libitum*. The welfare of the animals in the housing area and experiments conducted were in accordance with the Australian Code of Practice for the use of animals in research. All animal experimentation work was performed following approval by the Animal Ethics

Journal of Cell Science • Accepted manuscript

Committee, University of Sydney. Female mice between eight and twelve weeks of age were placed with a stud male overnight. The following morning the females were examined for a vaginal plug. Pregnant females with an observable vaginal plug were classed as 0.5 days pregnant. Pregnant mice were euthanised by cervical dislocation at developmental time points between embryonic day E8.5-18.5.

Generation of single cell suspensions from primary tissue

Mice were killed by cervical dislocation according to University of Sydney Animal Ethics Committee approval. Dissection and dissociation of brown and white gonadal adipose tissue for flow cytometric was performed as outlined previously (Boumelhem *et al.*, 2017). Brown adipose tissue was dissected from the interscapular region of the mouse while white adipose tissue was excised from the gonadal adipose depot. Skeletal muscle tissue (*bicep femoris*) was dissected from the quadriceps by bilateral incision. Liver, cardiac tissue, the adrenal gland and the testis were also excised for this study. Single cell suspensions of primary tissues were generated by mincing the tissues into fine pieces (~1-3 mm^3) in FACS buffer containing 0.1% (w/v) Collagenase Type II (Worthington) for 1 hour at 37°C with vigorous shaking every 15 minutes. Digested tissue was further dispersed with repeated pipetting followed by filtration through a 350 µm polystyrene mesh. An equal volume of FACS buffer was added to the filtered single cell suspension to inactivate the collagenase and then centrifuged for 5 minutes at 500 *g*. Centrifugation pellets the stromal vascular fraction (SVF) while the buoyant fraction containing adipocytes and lipid-containing cells float at the surface of the suspension.

Flow cytometric analyses of primary tissue

The buoyant fraction for each tissue was transferred to a separate 15 mL Corning tube whilst the SVF was resuspended in 1 mL of FACS buffer prior to staining. The SVF and buoyant fraction of each tissue was stained with FACS buffer containing 300 $nmol.L^{-1}$ of Nile Red and 2 $\mu mol.L^{-1}$ of Nile Blue for 15 minutes on ice. Multi-parametric flow cytometry was performed on a Gallios flow cytometer (Beckman Coulter, Brea, CA, USA) and data collected using the Kaluza G software package. FlowJo V10.1 was used to perform analyses of flow cytometric data. Two-tailed correlation analysis of the gated dataset was carried out in SPSS Statistics version 25 (IBM). Dimension reduction was performed using principal component analysis (PCA). Spanning-tree Progression Analysis of Density-Normalised Events (SPADE) was used to generate and group clusters of cells according to fluorescent antibody and probe staining properties (http://pengqiu.gatech.edu/software/SPADE/)[27].

Cryosectioning of primary tissues

All tissues assayed were placed in cryomolds (Tissue-Tek, The Netherlands), covered in optimal cutting temperature freezing medium (ProSciTech, Australia), placed in liquid nitrogen to snap freeze and stored at -80°C until needed. Frozen tissues were sectioned with a Leica CM1510S cryostat set at -15°C or -25°C for adipose tissue. All tissues were sectioned at 20 µm before being placed on a Superfrost glass slide (Menzel-Glaser, Germany).

Journal of Cell Science • Accepted manuscript

Confocal imaging of Nile Red and Nile Blue stained tissue

Tissue sections were fixed in 4% (v/v) PFA (in PBS) for 10-20 min at RT. Slides were then washed three times in PBS for five minutes each. Slides were stained with 300 nmol.L^{-1} Nile Red and 10 µmol.L^{-1} Nile Blue in a humidified chamber for 10 min. Slides were then washed twice with PBS for five minutes each and mounted in Vectashield containing DAPI (Vector Laboratories, USA). High resolution images were taken using a Zeiss LSM 800 confocal microscope coupled with the Zen Blue software package. Nile Red, Nile Blue and DAPI were excited at 488 nm, the 625 nm and the 405 nm lasers respectively. To detect and image Vitamin A fluorescence in sections of liver tissue, VectaShield mounting medium without DAPI was used as DAPI is excited at the same wavelength as Vitamin A (405 nm).

Statistical analyses

All data presented as mean ± SEM. Statistical analyses were performed using GraphPad Prism®. Comparisons between Nile Red and Nile Blue fluorescence in the presence of lipids was determined by a two-tailed, Student's *t*-test. Differences in Nile Red and Nile Blue fluorescence in the yolk sac at different stages of development were determined by one-way ANOVA with Tukey *post-hoc* multiple comparison test.

References

1. Frayn, K. N., Arner, P. & Yki-Järvinen, H. Fatty acid metabolism in adipose tissue, muscle and liver in health and disease. *Essays in Biochemistry* **42,** 89–103 (2006).

2. Rui, L. *Energy Metabolism in the Liver*. **97,** 177–197 (John Wiley & Sons, Inc., 2011).

3. Astakhova, L., Ngara, M., Babich, O., Prosekov, A., Asyakina, L., Dyshlyuk, L., Midtvedt, T., Zhou, X., Ernberg, I. & Matskova, L. Short Chain Fatty Acids (SCFA) Reprogram Gene Expression in Human Malignant Epithelial and Lymphoid Cells. *PLoS ONE* **11,** e0154102 (2016).

4. Hu, S., Dong, T.S., Dalal, S.R., Wu, Feng., Bissonnette, M., Kwon, J.H. & Change, E.B. The microbe-derived short chain fatty acid butyrate targets miRNA-dependent p21 gene expression in human colon cancer. *PLoS ONE* **6,** e16221 (2011).

5. Maekawa, M. & Fairn, G. D. Molecular probes to visualize the location, organization and dynamics of lipids. *Journal of Cell Science* **127,** 4801–4812 (2014).

6. Cespedes, E., Baylin, A. & Campos, H. Adipose tissue n-3 fatty acids and metabolic syndrome. *Eur J Clin Nutr* **69,** 114–120 (2015).

Journal of Cell Science • Accepted manuscript

7. Kerwin, J. L., Wiens, A. M. & Ericsson, L. H. Identification of fatty acids by electrospray mass spectrometry and tandem mass spectrometry. *J Mass Spectrom* **31,** 184–192 (1996).

8. Murphy, R. C. & Axelsen, P. H. Mass spectrometric analysis of long-chain lipids. *Mass Spectrom Rev* **30,** 579–599 (2011).

9. Smith, J. L. The staining of fat by Nile-blue sulphate. *Journal of Pathology and Bacteriology* **15,** 53–55 (1911).

10. Martinez, V. & Henary, M. Nile Red and Nile Blue: Applications and Syntheses of Structural Analogues. *Chemistry* **22,** 13764–13782 (2016).

11. Ostle, A. G. & Holt, J. G. Nile blue A as a fluorescent stain for poly-beta-hydroxybutyrate. *Appl. Environ. Microbiol.* **44,** 238–241 (1982).

12. Greenspan, P., Mayer, E. P. & Fowler, S. D. Nile red: a selective fluorescent stain for intracellular lipid droplets. *J. Cell Biol.* **100,** 965–973 (1985).

13. Rumin, J. The use of fluorescent Nile red and BODIPY for lipid measurement in microalgae. 1–16 (2015). doi:10.1186/s13068-015-0220-4

14. McMillian, M. K., Grant, E.R., Zhong, Z., Parker, J.B., Li, L., Zivin, R.A., Burczynski, M.E. & Johnson, M.D. Nile Red binding to HepG2 cells: an improved assay for in vitro studies of hepatosteatosis. *In Vitr Mol Toxicol* **14,** 177–190 (2001).

15. Dates, C. R., Fahmi, T., Pyrek, S.J., Yao-Borengasser, A., Borowa-Mazgaj, B., Bratton, S.M., Kadlubar, S.A., Mackenzie, P.I., Haun, R.S. & Radominska-Pandya, A. Human UDP-Glucuronosyltransferases: Effects of altered expression in breast and pancreatic cancer cell lines. *Cancer Biol. Ther.* **16,** 714–723 (2015).

16. Boumelhem, B. B., Assinder, S. J., Bell-Anderson, K. S. & Fraser, S. T. Flow cytometric single cell analysis reveals heterogeneity between adipose depots. *Adipocyte* **6,** 112–123 (2017).

17. Zwicker, V.E., Oliveira, B.L., Yeo, J.H., Fraser, S.T., Bernandes, G.J.L, New E.J. & Jolliffe, K. A Fluorogenic Probe for Cell Surface Phosphatidylserine Using an Intramolecular Indicator Displacement Sensing Mechanism. *Angewandte Chemie International Edition* **58, (10)** 3087-3091 (2019).

18. Lodhi, I. J. & Semenkovich, C. F. Peroxisomes: a nexus for lipid metabolism and cellular signaling. *Cell Metabolism* **19,** 380–392 (2014).

Journal of Cell Science • Accepted manuscript

19. Ahlabo, I. & Barnard, T. Observations of peroxisomes in brown adipose tissue of the rat. *J Histochem Cytochem* **19**(11), 670-5 (1971).

20. Park, H., He, A., Tan, M., Jordan, J.M., Dean, J.M., Pietka, T.A., Chen, Y., Zhang, X., Hsu, F-F., Razani, B., Katsuhiko, F. & Lohdi, I.J. Peroxisome-derived lipids regulate adipose thermogenesis by mediating cold-induced mitochondrial fission. *J Clin Invest* **129**(2), 694-711 (2019).

21. Farese, R. V., Cases, S., Ruland, S.L., Kayden, H.J., Wong, J.S., Young, S.G. & Hamilton, R.L. A novel function for apolipoprotein B: lipoprotein synthesis in the yolk sac is critical for maternal-fetal lipid transport in mice. *The Journal of Lipid Research* **37,** 347–360 (1996).

22. Rosol, T. J., Yarrington, J. T. & Latendresse, C. C. C. Adrenal gland: structure, function, and mechanisms of toxicity. *Toxicol Pathol* **29**(1), 41-8 (2001).

23. Griswold, M. D. Interactions between germ cells and Sertoli cells in the testis. *Biol. Reprod.* **52,** 211–216 (1995).

24. la Torre, de, B., Benagiano, G. & Diczfalusy, E. Pathways of testosterone synthesis in decapsulated testes of mice. *Acta Endocrinol.* **81,** 170–184 (1976).

25. Hu, J., Zhang, Z., Shen, W.-J. & Azhar, S. Cellular cholesterol delivery, intracellular processing and utilization for biosynthesis of steroid hormones. *Nutr Metab (Lond)* **7,** 47–25 (2010).

26. Campos-Silva, P., Furriel, A., Costa, W. S., Sampaio, F. J. B. & Gregorio, B. M. Metabolic and testicular effects of the long-term administration of different high-fat diets in adult rats. *Int Braz J Urol* **41,** 569–575 (2015).

27. O'Shaughnessy, P. J., Morris, I. D., Huhtaniemi, I., Baker, P. J. & Abel, M. H. Role of androgen and gonadotrophins in the development and function of the Sertoli cells and Leydig cells: data from mutant and genetically modified mice. *Molecular and Cellular Endocrinology* **306,** 2–8 (2009).

28. Zlobine, I., Gopal, K. & Ussher, J. R. Lipotoxicity in obesity and diabetes-related cardiac dysfunction. *Biochim. Biophys. Acta* **1861,** 1555–1568 (2016).

29. Higashi, N., Sato, M., Kojima, N., Irie, T., Kawamura, K., Mabuchi, A. & Senoo, H. Vitamin A storage in hepatic stellate cells in the regenerating rat liver: with special reference to zonal heterogeneity. *Anat Rec A Discov Mol Cell Evol Biol* **286,** 899–907 (2005).

Journal of Cell Science • Accepted manuscript

30. Qiu, P., Simonds, E.F., Bendall, S.C., Gibbs, K.D. Jr., Bruggner, R.V., Linderman, M.D., Sachs, K., Nolan, G.P. & Pievritis, S.K. Extracting a cellular hierarchy from high-dimensional cytometry data with SPADE. *Nat Biotechnol* **29,** 886–891 (2011).

31. Feldstein, A. E., Papouchado, B.G., Angulo, P., Sanderson, S., Adams, L. & Gores, G.J. Hepatic stellate cells and fibrosis progression in patients with nonalcoholic fatty liver disease. *Clin. Gastroenterol. Hepatol.* **3,** 384–389 (2005).

32. Li, J., Condello, S., Thomes-Pepin, J., Ma, X., Xia, Y., Hurley, T.D., Matei, D. & Cheng, J.X. Lipid Desaturation Is a Metabolic Marker and Therapeutic Target of Ovarian Cancer Stem Cells. *Cell Stem Cell* **20,** 303–314.e5 (2017).

33. Klouwer, F. C., Berendse, K., Ferdinandusse, S., Wanders, R.J., Engelen, M. & Poll-The, B.T. Zellweger spectrum disorders: clinical overview and management approach. *Orphanet J Rare Dis* **10,** 151–11 (2015).

34. Peake, K. B. & Vance, J. E. Defective cholesterol trafficking in Niemann-Pick C-deficient cells. *FEBS Letters* **584,** 2731–2739 (2010).

35. Kuo, Y. M., Zhou, B., Cosco, D., & Gitschier, J. The copper transporter CTR1 provides an essential function in mammalian embryonic development. *Pnas*, ***98***(12), 6836–6841 (2001).

Journal of Cell Science • Accepted manuscript

Figures

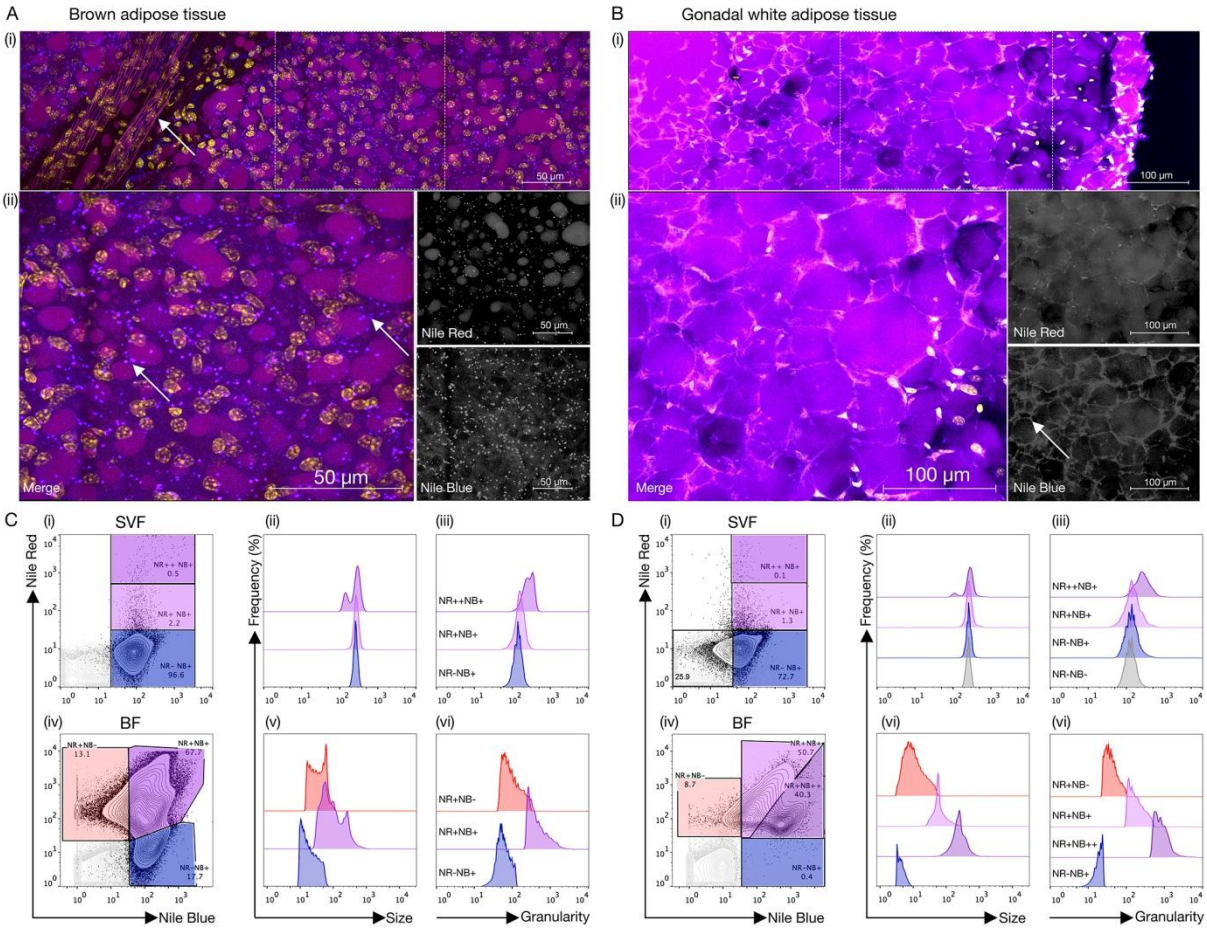

Fig. 1 Both Nile Blue and Nile Red are cell permeable, fluorescent lipophilic probes which fluoresce in mouse adipocytes

Representative images of cryosections (20 µm) of mouse (ai) brown and (bi) gonadal white adipose tissue stained with Nile Red (magenta), Nile Blue (blue) and DAPI (yellow) A z-stack of 20 µm was compiled for each sample. Images presented are a maximum intensity projection. Magnified regions (dotted box) of (aii) brown and (bii) gonadal white adipose tissue. White arrowhead in (ai) indicate Nile Red staining of laminar vessel-like structure. White arrowheads in (aii) and (bii) indicate Nile Blue staining of peroxisome-like structures. Single cell suspensions of (c) brown and (d) white adipose tissue were generated using the method previously published (Boumelhem *et al*., 2017). Cells of the stromal vascular fraction (SVF) (ci-iii, di-iii) and buoyant fraction (BF) (civ-vi, div-vi) were stained with Nile Red and Nile Blue and fluorescent populations identified. Gates were applied according to fluorescence intensity. Grey shaded region = unstained cells (NR-NB); red shaded region=-Nile Blue negative (NR+NB-); pink-shaded region =Nile Red negative, Nile blue positive cells (NR-NB+); Nile Red high, Nile Blue positive cells (NR++NB+, magenta); Nile Red and Nile Blue positive cells (NR+NB+). All populations were then back-gated to analyse the forward (size) (cii, dii) and side (granularity) (ciii, vi, diii,dvi) scatter profiles. For each cell preparation, at least 1 x 10^5 cells were analysed.

Journal of Cell Science • Accepted manuscript

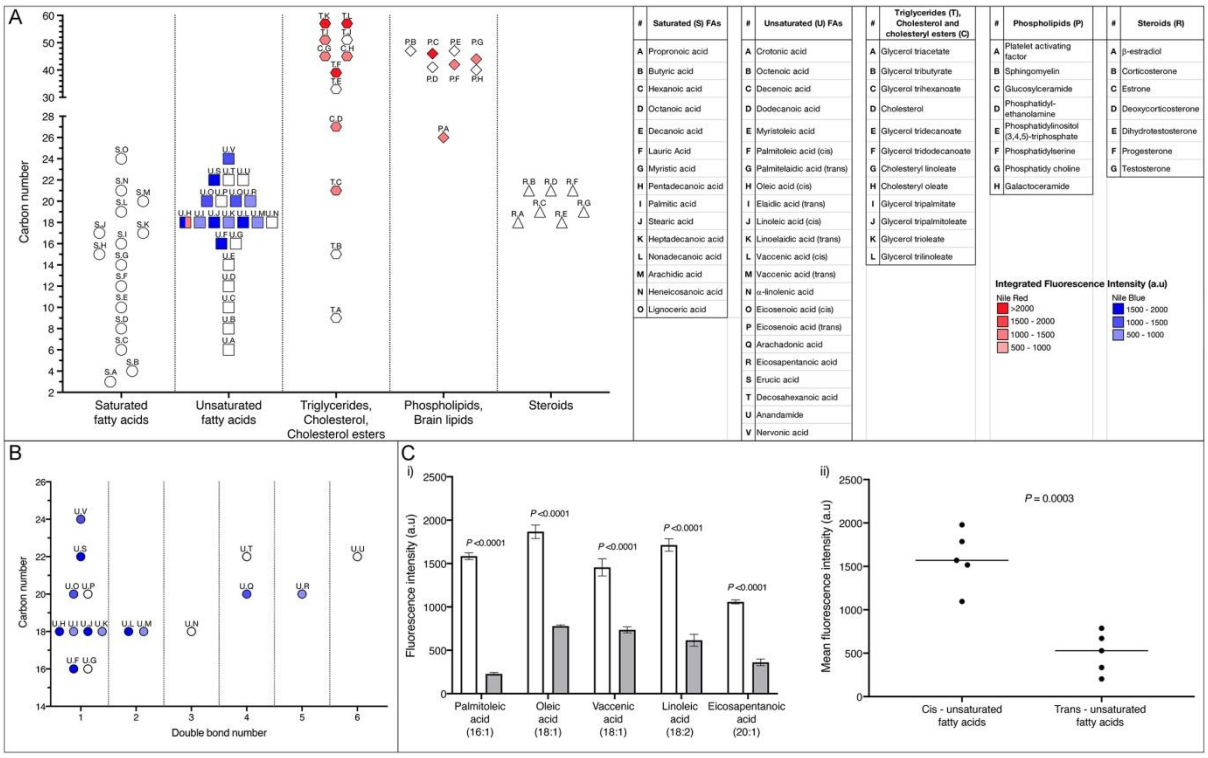

Fig. 2: Specificity of Nile Blue and Nile Red fluorescence in the presence of different lipid classes

Spectrofluorimetric analyses of (a); saturated (S) and unsaturated (U) fatty acids; triglycerides (T), cholesterol (C) and cholesterol esters (E); phospholipids (P) and brain (B) lipids and steroids (R) were performed in the presence of Nile Red and Nile Blue in PBS. Nile Red was excited at 488 nm while Nile Blue was excited at 620 nm. Emission was collected from 500 to 675 nm for Nile Red and 640 to 800 nm for Nile Blue. Integrated fluorescence intensity (a.u) presented as different shades of red (Nile Red) or blue (Nile Blue). (b) Comparisons between double bond number and carbon number of unsaturated fatty acids in the presence of Nile Blue. (ci-ii) Comparisons between *cis* (white bars) and *trans* (shaded bars) unsaturated fatty acids in the presence of Nile Blue. Data presented as mean ± SEM (n=3). Significant differences between *cis*- and *trans*-configured unsaturated fatty acids was determined using Student's *t*-test.

Journal of Cell Science • Accepted manuscript

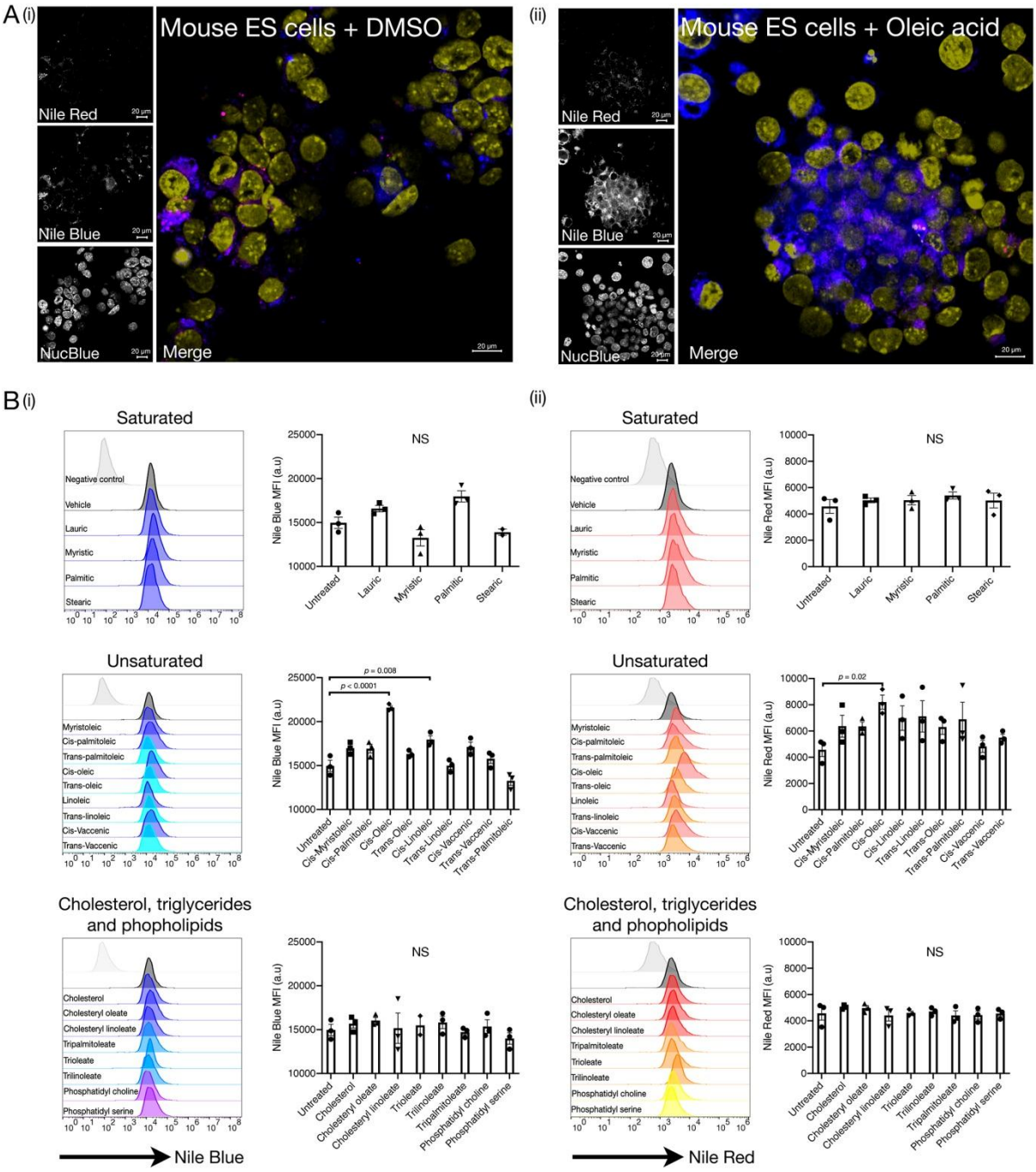

Fig. 3: Nile Blue and Nile Red preferentially stain oleic acid in live cells.

Representative images of mouse embryonic stem (ES) cells treated with DMSO (vehicle) (ai) or oleic acid (aii) and stained with Nile Red (magenta), Nile Blue (blue) and NucBlue (yellow) by confocal microscopy. Images were taken on a single plane. Scale bars represent 20 µm. (bi-ii)

Representative flow cytometric histogram plots of Nile Blue (bi) and Nile Red (bii) mean fluorescence intensity (MFI) in undifferentiated mouse ES cells treated with DMSO (vehicle – light grey); saturated free fatty acids, unsaturated free fatty acids, cholesterol, cholesterol

Journal of Cell Science • Accepted manuscript

esters, triglycerides and phospholipids. Data presented as mean ± SEM (n=3). Significance in Nile Blue and Nile Red fluorescence between lipids was determined by a two-tailed, one-way ANOVA with Tukey's *post hoc* multiple comparison test.

Journal of Cell Science • Accepted manuscript

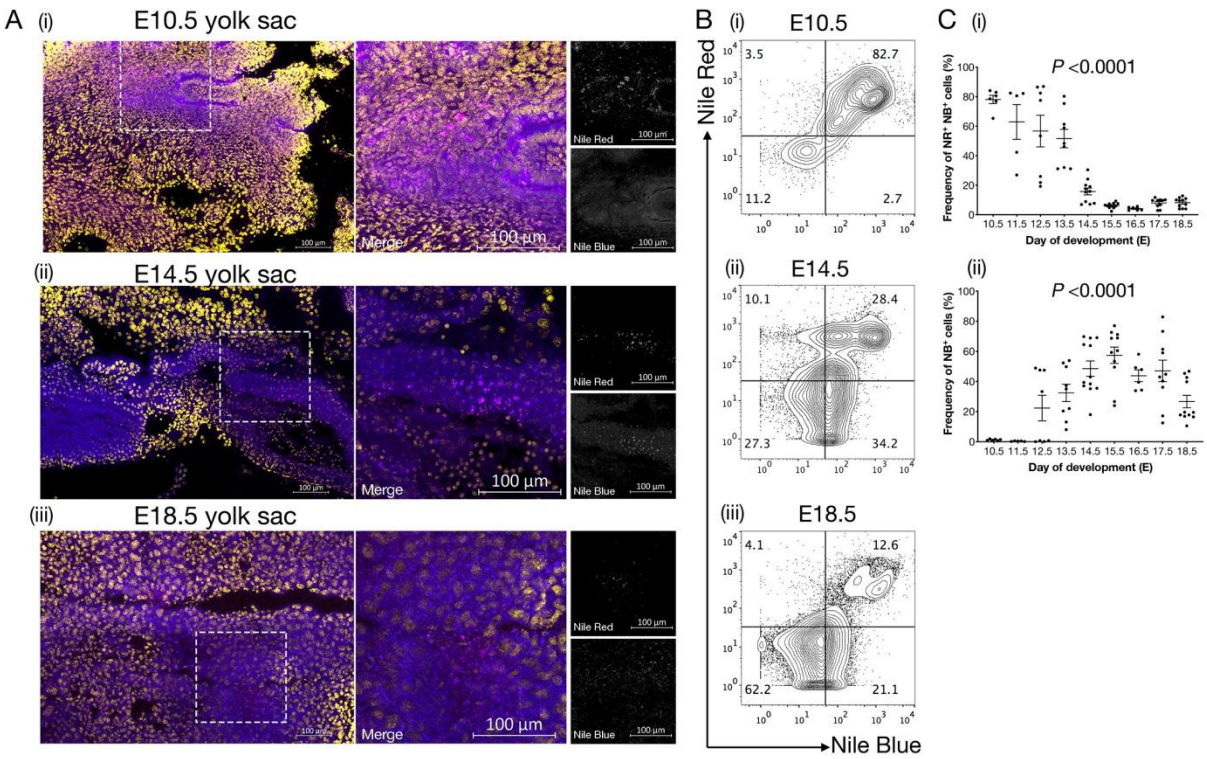

Fig. 4: Co-staining of Nile Blue and Nile Red reveals dynamic changes in the metabolism and transportation of lipids.

Representative images of 20 µm cryosections of mouse yolk sacs from embryos taken at embryonic day (a) (i) 10.5, (ii) 14.5 and (iii) E18.5, fixed with 4% PFA, stained with Nile Red (magenta), Nile Blue (blue) and DAPI (yellow) by confocal microscopy. A z-stack of 20 µm was compiled for each sample. Images presented are a maximum intensity projection.

Representative flow cytometric plots of (bi) E10.5, (ii) E14.5 and (iii) E18.5 yolk sacs stained with Nile Red and Nile Blue. Populations were gated according to Nile Red and Nile Blue fluorescence intensity.

(c) Comparison of (i) Nile Red and Nile Blue double positive cells (NR^+NB^+) and (ii) Nile Blue single positive cells (NB^+) in the yolk sacs of E10.5-E18.5 embryos (n=10 for each time point). Values presented are means ± SEM (n=2-5 independent experiments). Statistical significance was determined using a one-way ANOVA with Tukey *post-hoc* multiple comparison test (pairwise *P* values are given in Supplementary Tables 3 and 4).

Journal of Cell Science • Accepted manuscript

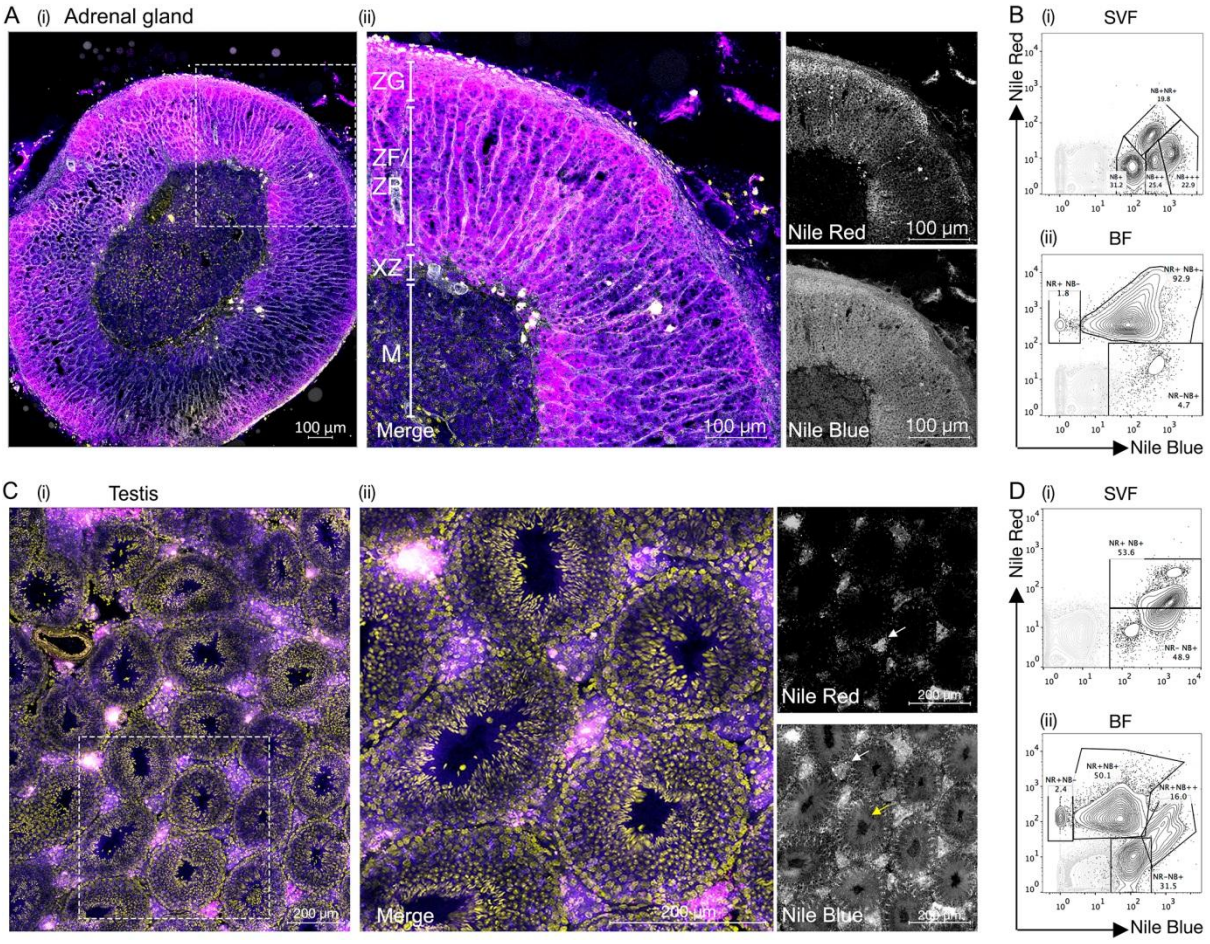

Fig. 5: Nile Blue and Nile Red double-staining identifies discrete populations in the mouse adrenal gland and testis.

Representative images of 20 µm cryosections of mouse (a) adrenal gland and (c) testis, fixed with 4% PFA, stained with Nile Red (magenta), Nile Blue (blue), phalloidin (adrenal only) (grey) and DAPI (yellow) by confocal microscopy. A z-stack of 20 µm was compiled for each sample. Magnified regions (white dotted box) of mouse (aii) adrenal gland and (cii) testis presented. ZG = zona glomerulosa, ZF = zona fasciculata, ZR = zona reticularis, XZ = z-zone and M = medulla. White arrowheads in (cii) represent Leydig cells. Yellow arrowheads highlight the seminiferous tubule.

Single cell suspensions of mouse (b) the adrenal gland and (d) testis were generated using the method previously published (Boumelhem *et al*., 2017). Cells of the stromal vascular fraction (SVF; ci, di) and buoyant fraction (BF; cii, dii) were stained with Nile Red and Nile Blue and fluorescence observed. Gates were applied according to fluorescence intensity: Nile Red positive (NR^{+}), Nile Blue positive (NB^{+}), Nile Red high (NR^{++}) or Nile Blue high (NB^{++}). For each cell fraction, at least 1 x 10^{5} cells were collected.

Journal of Cell Science • Accepted manuscript

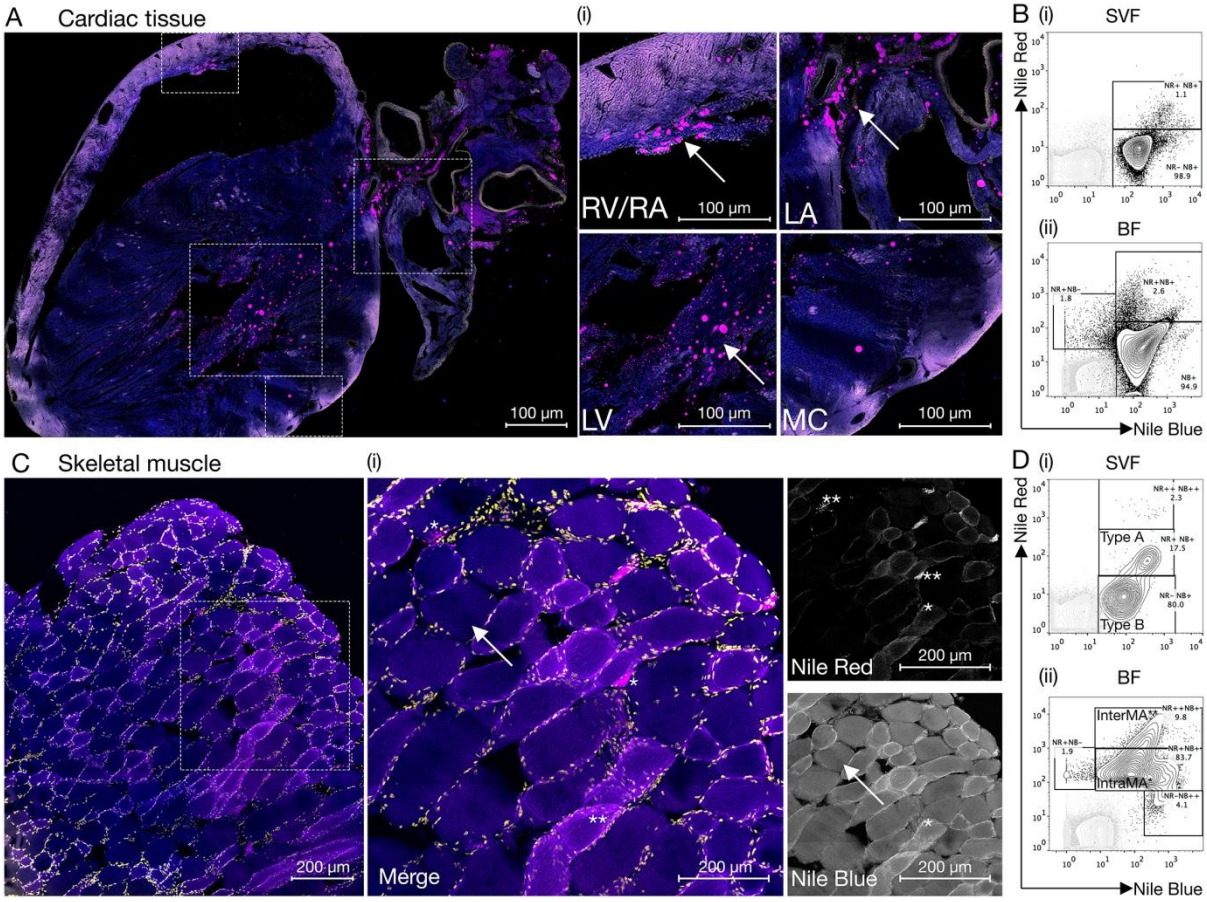

Fig. 6: Nile Blue and Nile Red co-staining highlights the distribution of lipids in mouse cardiac and skeletal muscle.

Representative images of 20 µm cryosections of mouse (a) heart tissue and (c) skeletal muscle (quadricep) were stained with Nile Red (magenta), Nile Blue (blue) and DAPI (yellow) by confocal microscopy. A tile-scan of 1,220 images were generated on a single plane for heart tissue. Magnified regions (dotted white boxes) of different areas of the mouse heart (ai) RV/RA = right ventricle/atrium; LA = left atrium; LV = left ventricle; MC = myocardium. Magnified regions (dotted white box) of skeletal muscle (ci). Arrowheads indicate different staining patterns of Nile Blue in skeletal muscle. Asterisks (* and **) representative of inter- and intramuscular adipocytes respectively. A z-stack of 20 µm was compiled for skeletal muscle and image projected is at maximum intensity.

Single cell suspensions of (b) heart tissue and (d) skeletal muscle were generated using the method previously published (Boumelhem *et al*., 2017). Cells of the stromal vascular fraction (SVF) and buoyant fraction (BF) were stained with Nile Red and Nile Blue and fluorescence observed. Two distinct populations (Type A and Type B) were distinguished by lipid contents in skeletal muscle. Gates were applied according to fluorescence intensity: Nile Red positive (NR^{+}), Nile Blue positive (NB^{+}), Nile Red high (NR^{++}) or Nile Blue high (NB^{++}). Putative identity for the most frequent cell type is included. For each cell preparation, at least 1 x 10^{5} cells were collected.

Journal of Cell Science • Accepted manuscript

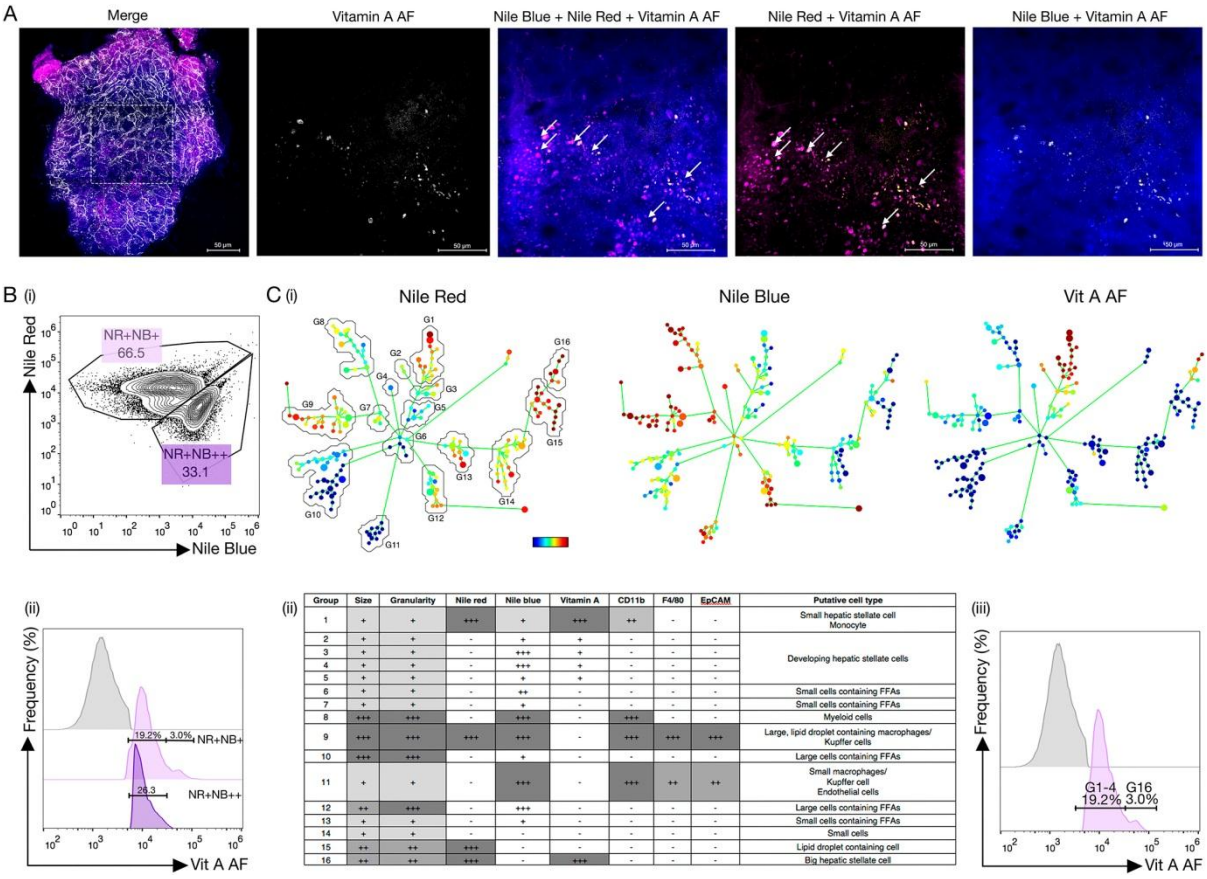

Group	Size	Granularity	Nile red	Nile blue	Vitamin A	CD11b	F4/80	EpCAM	Putative cell type
1	+	+	+++	+	+++	++	-	-	Small hepatic stellate cell Monocyte
2	+	+	-	+	+	-	-	-	Developing hepatic stellate cells
3	+	+	-	+++	+	-	-	-	
4	+	+	-	+++	+	-	-	-	
5	+	+	-	+	+	-	-	-	
6	+	+	-	++	-	-	-	-	Small cells containing FFAs
7	+	+	-	+	-	-	-	-	Small cells containing FFAs
8	+++	+++	-	+++	-	+++	-	-	Myeloid cells
9	+++	+++	+++	+++	-	+++	+++	+++	Large, lipid droplet containing macrophages/ Kupffer cells
10	+++	+++	-	+	-	-	-	-	Large cells containing FFAs
11	+	+	-	+++	-	+++	++	++	Small macrophages/ Kupffer cell Endothelial cells
12	++	+++	-	+++	-	-	-	-	Large cells containing FFAs
13	+	+	-	+	-	-	-	-	Small cells containing FFAs
14	+	+	-	-	-	-	-	-	Small cells
15	++	++	+++	-	-	-	-	-	Lipid droplet containing cell
16	++	++	+++	-	+++	-	-	-	Big hepatic stellate cell

Fig. 7: Multiparametric analyses reveals differences in the distribution of lipids in the mouse liver.

(a) Representative image of 20 µm cryosection of mouse liver with Nile Red (magenta), Nile Blue (blue), Vitamin A autofluorescence (yellow) and phalloidin (white) by confocal microscopy. Nile Red and phalloidin were excited at 488 nm; Nile Blue was excited at 620 nm and Vitamin A was excited at 408 nm. A z-stack of 20 µm was compiled and image projected is at maximum intensity. White arrowheads represent Hepatic Stellate Cells.

(b) Single cell suspensions of mouse liver were generated using the method previously published (Boumelhem *et al.*, 2017). Cells of the BF were stained with Nile Red and Nile Blue and fluorescence observed. Gates were applied according to Nile Red and Nile Blue fluorescence intensity and Vitamin A autofluorescence measured in each population. Light purple gated population represents Nile Red positive (NR^{+}), Nile Blue positive (NB^{+}) cells while the dark purple gated population represents the Nile Red positive (NR^{+}), Nile Blue High (NB^{++}) cells. Grey histogram peak is representative of the Vitamin A negative population.

(ci) Multiparametric, 'Spanning-tree Progression Analysis of Density-Normalised Events' (SPADE) (Qiu *et al.*, 2011) analyses on the BF of dissociated hepatic tissue. Each node represents a cluster of cells. Blue coloured nodes indicate low levels of fluorescence for that marker while red indicates high levels of fluorescence. Clusters of nodes were grouped together according to differences in fluorescence intensity. Vitamin A autofluorescence was

Journal of Cell Science • Accepted manuscript

measured in the entire BF of dissociated hepatic tissue and gates applied according to fluorescence intensity. (cii) Representative groups (G1-16) of the BF according to fluorescence intensity of each parameter and putative cell identity based on fluorescent signals. (cii) Gated populations in the histogram plot are representative of groups 1-4 and group 16 of the SPADE plot.

Journal of Cell Science • Accepted manuscript

Table S1. List of fatty acids assayed in this study. Peak emission (λ_{max}) presented as mean ± SEM (n=3).

Name	Class	C atom #	DB #	ω-pos	Nile Blue λ_{max} 660 nm	Nile Red λ_{max} 575 nm
Cholesterol	Cholesterol	27	1	-	171 ± 4	597 ± 15
Cholesteryl linoleate	Cholesterol ester	45	2	-	281 ± 5	989 ± 22
Cholesteryl oleate	Cholesterol ester	45	3	-	197 ± 8	1230 ± 20
1-oleoyl-2-sn-2-glycerol	Diglyceride	37	0	-	154 ± 10	781 ± 16
Galactoceramide	Phospholipid	40	1	-	130 ± 4	200 ± 14
Glucosylceramide	Phospholipid	46	1	-	603 ± 30	2574 ± 150
L-a-phosphatidyl choline	Phospholipid	42	2	-	437 ± 15	1086 ± 40
Platelet activating factor (PAF)	Phospholipid	26	0	-	451 ± 50	1244 ± 53
Phosphatidyl ethanolamine	Phospholipid	41	2	-	315 ± 14	155 ± 6
Phosphatidyl serine	Phospholipid	42	2	-	480 ± 30	647 ± 26
Phosphatidylinositol (3,4,5)-triphosphate	Phospholipid	47	4	-	130 ± 9	40 ± 2
Sphingomyelin	Phospholipid	47	2	-	160 ± 6	322 ± 22
Myelin basic protein	Protein	-	-	-	134 ± 8	248 ± 5
High density lipoprotein	Protein	-	-	-	1038 ± 44	1289 ± 50
Low density lipoprotein	Protein	-	-	-	661 ± 26	2076 ± 70
Propionic Acid	Saturated	3	0	-	47 ± 3	96 ± 5
Glycerol	Saturated	3	0	-	111 ± 5	120 ± 12
O-phosphorylethanolamine	Saturated	3	0	-	100 ± 5	100 ± 8
Butyric acid	Saturated	4	0	-	282 ± 10	35 ± 2
Hexanoic acid	Saturated	6	0	-	127 ± 8	55 ± 6
D-galactose	Saturated	6	0	-	130 ± 12	135 ± 20
Decanoic acid	Saturated	10	0	-	52 ± 2	119 ± 24
Lauric Acid	Saturated	12	0	-	20 ± 1	10 ± 1
Myristic acid	Saturated	14	0	-	18 ± 2	110 ± 14
Pentadecanoic acid	Saturated	15	0	-	144 ± 6	154 ± 19
Palmitic acid	Saturated	16	0	-	92 ± 4	276 ± 25
Stearic acid	Saturated	17	0	-	107 ± 4	103 ± 10
Heptadecanoic acid	Saturated	17	0	-	361 ± 15	122 ± 10
Nonadecanoic acid	Saturated	19	0	-	37 ± 2	65 ± 4
Arachidic acid	Saturated	20	0	-	414 ± 15	53 ± 4
Heneicosanoic acid	Saturated	21	0	-	91 ± 6	37 ± 5
Lignoceric acid	Saturated	24	0	-	53 ± 4	18 ± 4
Octanoic acid	Saturated	8	0	-	14 ± 1	72 ± 10
Triacetate	Saturated - triglyceride	9	0	-	88 ± 10	120 ± 11
Tributyrate	Saturated - triglyceride	15	0	-	120 ± 15	164 ± 14

Trihexanoate	Saturated - triglyceride	21	0	-	73 ± 9	1186 ± 91
Tridecanoate	Saturated - triglyceride	33	0	-	138 ± 12	3065 ± 180
Tridodecanoate	Saturated - triglyceride	39	0	-	82 ± 8	319 ± 29
Tripalmitate	Saturated - triglyceride	51	0	-	41 ± 3	540 ± 33
Tripalmitoleate	Saturated - triglyceride	51	3	7	203 ± 17	3515 ± 220
Trioleate	Saturated - triglyceride	57	3	9	175 ± 19	2121 ± 159
Trilinoleate	Saturated - triglyceride	57	6	9	70 ± 5	1412 ± 144
Oestrogen	Steroid	18	3	-	66 ± 4	53 ± 3
Estrone	Steroid	18	3	-	31 ± 3	147 ± 6
Dihydrotestosterone	Steroid	19	0	-	161 ± 6	282 ± 10
Testosterone	Steroid	19	0	-	102 ± 4	137 ± 8
Corticosterone	Steroid	21	1	-	154 ± 5	32 ± 2
Deoxycorticosterone	Steroid	21	1	-	120 ± 5	149 ± 9
Progesterone	Steroid	21	1	-	76 ± 2	147 ± 8
Crotonic acid	Unsaturated	4	1	2	111 ± 9	21 ± 1
7-Octenoic acid	Unsaturated	8	1	5	136 ± 5	37 ± 1
2-Decenoic acid	Unsaturated	10	1	5	90 ± 10	50 ± 2
5-Dodecanoic acid	Unsaturated	12	1	7	71 ± 5	117 ± 10
Myristoleic acid	Unsaturated	14	1	5	36 ± 2	37 ± 2
Palmitoleic acid	Unsaturated	16	1	7	1585 ± 41	193 ± 5
Linoleic acid	Unsaturated	18	2	6	1713 ± 67	142 ± 9
Oleic acid	Unsaturated	18	1	9	1867 ± 59	600 ± 30
a-linolenic acid	Unsaturated	18	3	6	244 ± 22	217 ± 15
Cis-vaccenic acid	Unsaturated	18	1	7	1455 ± 35	361 ± 19
Arachadonic acid	Unsaturated	20	4	6	1338 ± 29	348 ± 22
Eicosenoic acid	Unsaturated	20	1	9	1057 ± 49	210 ± 11
Eicosapentanoic acid	Unsaturated	20	5	3	663 ± 25	244 ± 14
1-monooleoyl-rac-glycerol	Unsaturated	21	1	9	130 ± 8	30 ± 2
Erucic acid	Unsaturated	22	1	9	1650 ± 85	335 ± 10
Decosahexanoic acid	Unsaturated	22	6	3	418 ± 45	234 ± 11
Anandamide	Unsaturated	22	4	6	178 ± 24	525 ± 45
Nervonic acid	Unsaturated	24	1	9	894 ± 37	298 ± 29
Palmitelaidic acid	Unsaturated - trans	16	1	7	228 ± 11	109 ± 4
Elaidic acid	Unsaturated - trans	18	1	9	779 ± 38	187 ± 14
Linoelaidic acid	Unsaturated - trans	18	2	6	529 ± 15	62 ± 9
Trans-vaccenic acid	Unsaturated - trans	18	1	7	716 ± 18	303 ± 16
11(E)-Eicosenoic acid	Unsaturated - trans	20	1	9	360 ± 11	91 ± 10
Mineral oil		-	-	-	5 ± 1	1237 ± 122

Table S2. ***Pairwise comparisons of changes in Nile Red fluorescence in the yolk sac across development. P values given, NS = non significant difference.***

Embryonic day (E)	10.5	11.5	12.5	13.5	14.5	15.5	16.5	17.5	18.5
10.5		*NS*	*NS*	*NS*	*<0.0001*	*<0.0001*	*<0.0001*	*<0.0001*	*<0.0001*
11.5			*NS*	*NS*	*<0.0001*	*<0.0001*	*<0.0001*	*<0.0001*	*<0.0001*
12.5				*NS*	*<0.0001*	*<0.0001*	*<0.0001*	*<0.0001*	*<0.0001*
13.5					*<0.0001*	*<0.0001*	*<0.0001*	*<0.0001*	*<0.0001*
14.5						*NS*	*NS*	*NS*	*NS*
15.5							*NS*	*NS*	*NS*
16.5								*NS*	*NS*
17.5									*NS*
18.5									

Table S3. ***Pairwise comparisons of changes in Nile Blue fluorescence in the yolk sac across development. P values given, NS = non significant difference.***

Embryonic day (E)	10.5	11.5	12.5	13.5	14.5	15.5	16.5	17.5	18.5
10.5		*NS*	*NS*	*0.0195*	*<0.0001*	*<0.0001*	*0.0012*	*<0.0001*	*NS*
11.5			*NS*	*0.0261*	*<0.0001*	*<0.0001*	*0.0018*	*<0.0001*	*NS*
12.5				*NS*	*0.0111*	*0.0008*	*NS*	*NS*	*NS*
13.5					*NS*	*0.0357*	*NS*	*NS*	*NS*
14.5						*NS*	*NS*	*NS*	*0.0245*
15.5							*NS*	*NS*	*0.0016*
16.5								*NS*	*NS*
17.5									*NS*
18.5									

Journal of Cell Science • Supplementary information

Table S4. Principal component analysis correlation matrix for data presented in adult mouse liver SPADE analysis. Significance (1-tailed): * $p<0.05$; ** $p<0.01$

	FSC	SSC	CD11b	NR	PI	EpCAM	NB	F4/80	VitA
Size		*0.546***	*0.247***	*0.061*	*-0.017*	*0.120**	*0.276***	*0.005*	*0.317***
Granularity			*0.356***	*0.635**	*0.287***	*0.240***	*0.641***	*0.137**	*0.844***
CD11b				*0.117**	*-0.422***	*0.232***	*0.520***	*0.204***	*0.560***
NR					*0.501***	*0.349***	*0.501***	*0.301***	*0.747***
PI						*0.202***	*0.231***	*-0.013*	*0.255***
EpCAM							*0.367***	*0.614***	*0.366***
NB								*-0.006*	*0.801***
F4/80									*0.210***
VitA									

Table S5. Fluorescently-conjugated antibodies used for multiparametric flow cytometric analyses in the mouse liver.

Antibody	Fluorophore	Cat #	Clone	Source	Citation
Anti-mouse F4/80	APC	123115	BM8	BioLegend	Schaller, E *et al*. *Mol. Cell. Biol.* 22:8035. (2002)
Anti-mouse CD326 (EpCAM)	PerCP/Cyanine 5.5	118219	G8.8/	BioLegend	Dooley, J *et al*. *J Immunol.* 175:4331. (2005).
Anti-mouse/human CD11b	FITC	101205	M1/70	BioLegend	Iwasaki, A and Kelsall, B. L. 2001. *J. Immunol.* 166:4884 (2001).

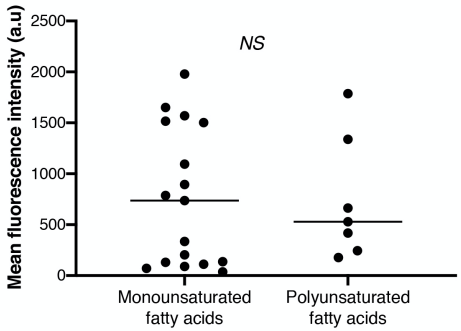

Figure S1: No differences in Nile Blue fluorescence between mono- and polyunsaturated fatty acids.
Spectrofluorimetric analyses of unsaturated fatty acids in the presence of Nile Blue comparing mono- and polyunsaturated fatty acids. Fatty acids were reconstituted in DMSO and pipetted onto a 96-well plate at a final concentration of 100 µmol.L^{-1}. Nile Blue was added to a final concentration of 1 µmol.L^{-1} and excited at 620 nm. Emission was collected from 640 to 800 nm. Data presented as mean ± SEM (n=3). Significant differences between monounsaturated and polyunsaturated fatty acids were determined by Students *t*-test.

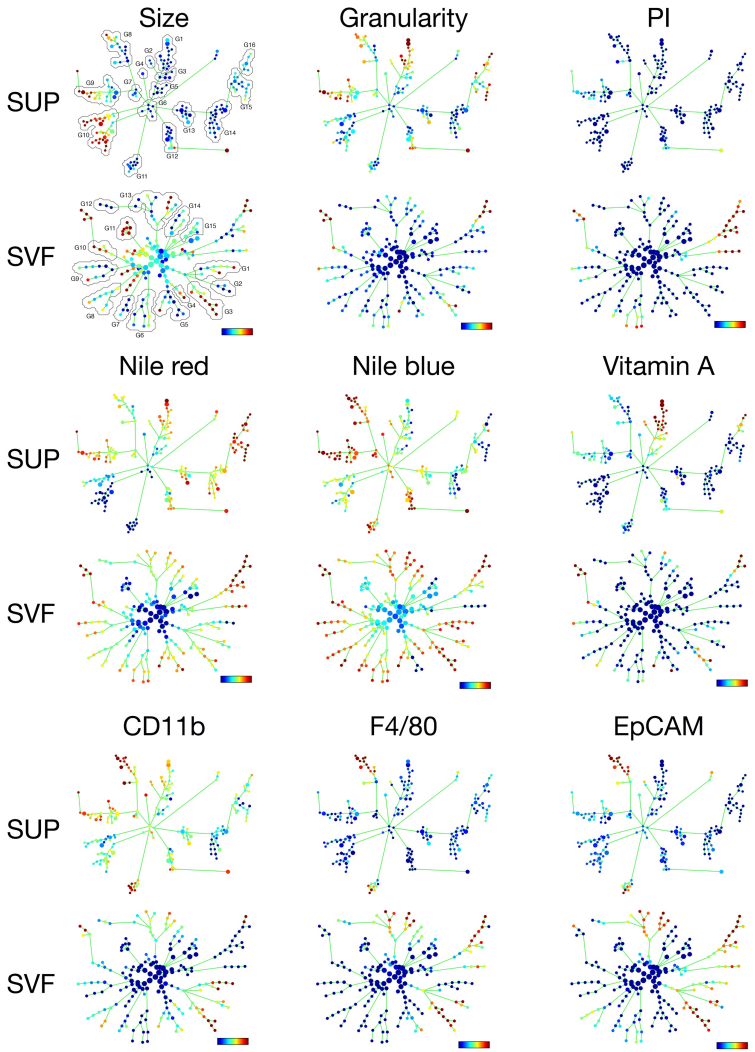

Figure S2: Multiparametric, flow cytometric analyses of hepatic tissue organised by SPADE plots distinguish clusters of lipid rich populations.
Spanning-tree Progression Analysis of Density-Normalised Events' (SPADE)[80] analyses were conducted on the buoyant fraction (BF) and stromal vascular fraction (SVF) of dissociated mouse livers stained with Nile Red, Nile Blue, F4/80, EpCAM, CD11b and propidium iodide. Side scatter (granularity), forward scatter (size) and propidium iodide (PI) were also used to build the SPADE tree consisting of a total of 200 nodes. Each node represents a cluster of cells. Blue coloured nodes indicate low levels of fluorescence for the respective marker while red indicates high levels of fluorescence. Clusters of nodes were grouped together according to differences in fluorescence intensity.

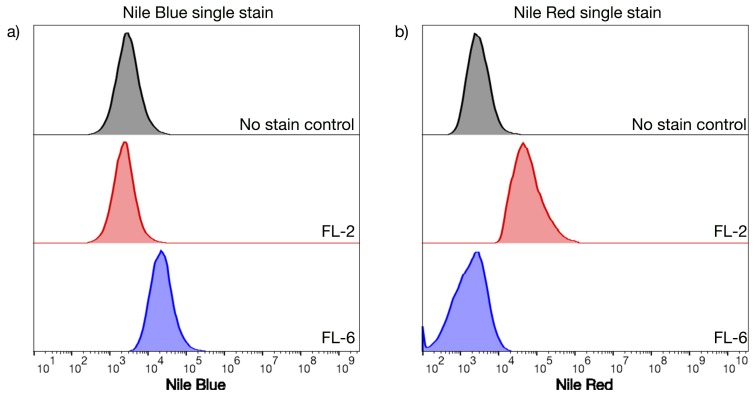

Figure S3: Nile Blue and Nile Red do not overlap in spectral emission by flow cytometry. Single cell suspensions of white adipose tissue were generated using the method previously published[16]. Cells of the buoyant fraction were stained with either Nile Blue (a) or Nile Red (b) and fluorescent populations identified. Fluorescent channel (FL) 6 is excited by the 620 nm laser and detects emission at 660 ± 20 nm. Fluorescent channel (FL) 2 is excited by the 488 nm laser and detects emission at 575 ± 30 nm. Nile Blue (blue shaded plot) and Nile Red (red shaded plot) are only detected in the FL-6 and FL-2 respectively. The black shaded plot represents the no-stain control.

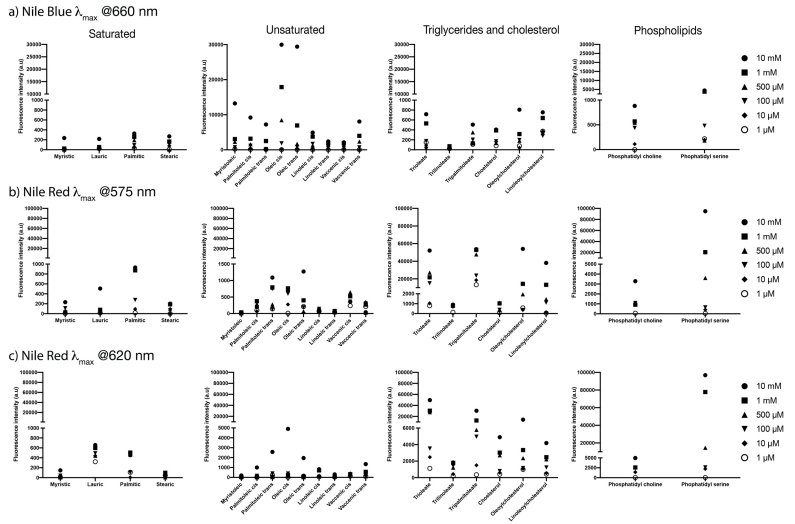

Figure S4: Increasing lipid concentration elicits greater Nile Blue and Nile Red fluorescence.
Spectrofluorimetric analyses of lipids from multiple classes (saturated and unsaturated free fatty acids, cholesterol, cholesterol esters, triglycerides and phospholipids) were performed in the presence of Nile Blue and Nile Red. A dose-response was performed to determine the relationship between lipid concentration and Nile Blue and Nile Red fluorescence. The concentration of lipids ranged from 1 µM - 10 mM. Nile Blue was excited at 620 nm while Nile Red was excited at 488 nm. Peak emission (λ_{max}) for Nile Blue (a) was collected at 660 nm; at 575 nm (b) and 620 nm (c) for Nile Red.